Dual-functional crystalline BeO layer in enhancement-mode ZnO/Si thin film transistors

Huili Liang[*,1], **Zengxia Mei**[**,1], **Daqian Ye**[1], **Junqiang Li**[1], **Wen-Chiang Hong**[2], **Qinghua Zhang**[3], **Yaoping Liu**[1], **Lin Gu**[3], **Richeng Yu**[3], **Yicheng Lu**[2], and **Xiaolong Du**[1]

[1] Key Laboratory for Renewable Energy, Beijing National Laboratory for Condensed Matter Physics, Institute of Physics, Chinese Academy of Sciences, P. O. Box 603, Beijing 100190, P.R. China

[2] Department of Electrical and Computer Engineering, Rutgers University, 94 Brett Road, Piscataway, NJ 08854, USA

[3] Key Laboratory of Advanced Materials and Electron Microscopy, Beijing National Laboratory for Condensed Matter Physics, Institute of Physics, Chinese Academy of Sciences, P. O. Box 603, Beijing 100190, P.R. China

* Corresponding author: e-mail hlliang@iphy.ac.cn, Phone: +86 10 8264 8062, Fax: +86 10 8264 9975
** e-mail zxmei@iphy.ac.cn

Integration of oxides with Si opens promising opportunities for novel multifunctional devices and new applications. To optimize the device performances through the hybrid integration, keeping the oxide/Si interface abrupt is critically important and challenging due to the seemingly unavoidable formation of amorphous SiO_x or silicide interfacial layers. Here, we report an interface-engineering approach to this issue by molecular beam epitaxy. A BeO thin layer ($\sim$5 nm) was deposited on Si (111) surface using a two-step process of Be deposition and oxidation. The initially formed BeO served as a template for subsequent homo-epitaxial growth of a 10-nm crystalline BeO layer. The well-defined interface between BeO and Si is clearly discerned by high-resolution transmission electron microscopy, implying the role of crystalline BeO as a barrier layer against oxygen atoms' diffusion. High-resolution X-ray photoelectron spectroscopy further confirmed that the combined BeO layers sufficiently protect the Si surface from oxidation. A bottom-gate enhancement-mode thin film transistor was established on a ZnO (130 nm)/BeO (70 nm)/ Si architecture, where BeO was functionalized both as a diffusion barrier and as a high-*k* gate insulator. It indicates that this methodology can be potentially extended to hybrid integration of other technologically important crystalline oxides with Si infrastructures.

1 Introduction Crystalline oxides on Si (COS) [1–4], with the combined advantages of oxides' multi-functionality and highly-developed Si infrastructures, have been considered as desirable replacements for SiO_2 to further extend and enhance Si technology [5]. The COS enables new device physics with preserving translational symmetry in an atomic scale level [6], where it is critically important to keep the oxide/Si interface abrupt for the optimal device performance. However, Si is reactive with many elements, especially oxygen, resulting in extensive inter-diffusion or chemical reactions. The readily formed amorphous SiO_x layer and metal silicates will not only interrupt the translational symmetry at the interface, but also hinder the highest achievable gate capacitance. Consequently, an effective scheme to overcome these obstacles is highly desired.

Many groups have devoted themselves to breaking this bottleneck. To decrease the oxide-Si interface mixture and reaction, some researchers deposited oxides at advisedly selected temperatures with compromise of the crystallinity [7–9]. Nevertheless, SiO_x, silicates or silicides would still frequently appear at the interface after high-temperature growth or post-annealing treatment aiming to improve the oxide crystal quality [7–9]. Some other crystalline oxides such as $MgAl_2O_4$ [10], Al_2O_3 [11], Gd_2O_3 [12], and Sc_2O_3 [13], which seem to be thermally stable when contacting with Si, were deposited on clean Si surface in attempt to form COS structures. However, high

density of defects originating from domain boundaries or lattice reorientation often existed in these oxide films, which could provide channels for the leakage current, thus degrading the dielectric properties. Therefore, new material systems need to be explored. According to the metal/Si binary phase diagrams, Be/Si appears attractive with the virtue of no mutual solubility or intermediate reaction even at a temperature as high as 1085 °C [14]. The thermodynamic study conducted by K. J. Hubbard and D. G. Schlom indicates that BeO/Si contact is stable even at 700 °C [15]. Due to the small Be-O length (1.686 Å along c-axis) and its interstitial size, BeO is expected to be an effective diffusion barrier against oxygen and other atoms to maintain an abrupt interface with Si [16]. A BeO thin film has a higher dielectric constant ($k = 6.75 \pm 0.08$) [17] than SiO_2 ($k = 3.8073$) [18] and possesses the desirable conduction and valence band offsets with respect to Si ($\Delta E_c = 2.6 \pm 0.1$ eV and $\Delta E_v = 4.14 \pm 0.2$ eV) [19]. The new Be-based oxide material system shows promise in high-quality COS structures, providing an alternative solution to replace the popular SiO_2 dielectrics. In previous report, BeO layer has been deposited on Si (100) by atomic layer deposition (ALD) technique [15]. However, its crystal structure was mixed phases with wurtzite and zinc-blende, demonstrating that the hetero-epitaxial growth of oxides on Si cannot be directly initiated with the oxide layer, and interface engineering is essential for the achievement of high quality COS structures.

Considering both the crystal structures of Be ($a = 2.286$ Å, $c = 3.584$ Å, PDF #22-0111) and BeO ($a = 2.698$ Å, $c = 4.378$ Å, PDF #35-0818) are hexagonal with six-fold symmetry, while Si atoms configure like hexagonal honeycomb on (111) surface with the nearest distance about 3.840 Å ($a = 5.431$ Å, PDF #27-1402), Si(111) surface was chosen in this work. An *in situ* oxidation process of the Be (0001)/Si (111) system was performed by radio-frequency plasma assisted molecular beam epitaxy (rf-MBE) technique, which assured a deliberately-engineered BeO/Si interface in an atomic-layer precision level. The initially formed BeO served as a template for subsequent homo-epitaxial growth of 10-nm crystalline BeO layer. No signal from Si–O bond was detected in high-resolution X-ray photoelectron spectroscopy (HRXPS) measurements, indicating that combination of these two BeO layers can sufficiently protect Si surface from oxidation in the active oxygen radicals. A bottom-gate thin film transistor (BG-TFT) was realized using the structure of ZnO (130 nm)/BeO (70 nm)/Si. The 70-nm BeO layer not only served as a diffusion barrier but also a high-k gate insulator. The TFT clearly works in the enhancement mode, resulting from the low background electron concentration in the epitaxial ZnO channel.

2 Experimental Be (0001) thin layers with a thickness of ∼5 nm were synthesized on Si (111) substrates by rf-MBE technique with a background pressure of ∼1×10^{-7} Pa. The wafer was chemically cleaned by the regular RCA method and then thermally cleaned at high temperature under ultrahigh vacuum (UHV) condition. Elemental Be (4N) was evaporated by Knudsen cells (Veeco). The subsequent *in situ* oxidation process was performed using radical oxygen (5.5N) generated by rf-plasma system (SVTA) to form the crystalline BeO template layer (TL). Reflection high energy electron diffraction (RHEED) technique was efficiently utilized to *in situ* monitor the whole growth process and the crystal phase evolutions. Surface morphology and roughness of the film was evaluated by using commercial Atomic force microscopy (AFM, SPA-400, SIINT) with contact mode tips (OMCL-TR400PSA, Olympus). The specific interfacial structure was explored by the cross-sectional high resolution transmission electron microscopy (HRTEM) in a Tecnai F20 ST transmission electron microscope operated at 200 kV equipped with a Gatan filter system. The cross-sectional samples with a single-crystal ZnO capping layer were thinned to electron transparency by mechanically polishing and Ar ion milling.

To confirm the effectiveness of BeO as a diffusion barrier in keeping an abrupt oxide/Si interface, a 10 nm BeO thin layer was homo-epitaxially grown on the interface-engineered BeO TL. To further investigate the crystal structure of the BeO thin layer, grazing incidence X-ray diffraction (GIXRD) was carried out using a light source ($\lambda = 1.5482$ Å) from synchrotron radiation in Beijing Synchrotron Radiation Facility (BSRF). The chemical bond states of Be and Si at the interface were determined by XPS, which was carried out in a scanning XPS microprobe system (ESCALAB 250xi, Thermo Fisher Scientific) with a background pressure of 3.4×10^{-10} mbar.

BG-TFT devices were fabricated on the structure of ZnO (130 nm)/BeO (70 nm)/Si. The ZnO channel layer was patterned by hydrochloric acid. Then a bilayer of 90-nm-thick titanium and 60-nm-thick gold as source and drain electrodes was deposited by thermal evaporation and patterned through lift-off process. The size of the active layer is fixed at a width/length (W/L) = 150 μm/5 μm.

3 Results and discussion
3.1 Preparation and properties of oxidized BeO TL on Si Figure 1a and b show the *in situ* RHEED patterns of the Si (111) surface after chemically cleaning and thermally cleaning (at 800 °C), respectively. A clear 7×7 reconstruction pattern in Fig. 1b indicates that the native SiO_x layer has been successfully removed. Figure 1c is the RHEED patterns of a 5 nm Be thin layer deposited at 200 °C. It can be deduced from the comparison of Figure 1b and c that the epitaxial relationship between the Be layer and Si substrate is (0001)Be[0001]//(111)Si[111] and ($10\bar{1}0$) Be [$10\bar{1}0$] //($10\bar{1}$) Si [$10\bar{1}$]. The top view of the Be atoms on Si (111) surface is schematically shown in Fig. 1d. As indicated in Fig. 1d, the nearest distance of Si atoms on (111) surface is 3.840 Å (in the following parts, we will use the equation $\alpha_{Si}(111) = 3.840$ Å), while on Be (0001) surface, the nearest distance of Be atoms is 2.286 Å. In such

Phys. Status Solidi RRL 11, No. 5 (2017)

Rapid
Research Letter

(3 of 8) 1600443
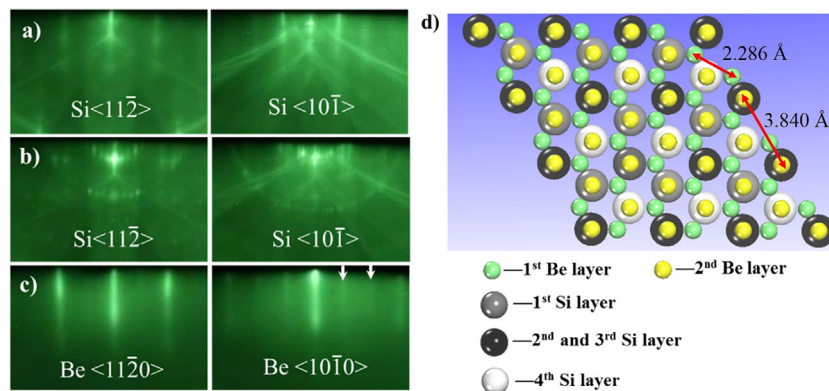
Figure 1 RHEED patterns with incident electron beams along $\langle 11\bar{2} \rangle_{Si}$ and $\langle 10\bar{1} \rangle_{Si}$ azimuths, respectively, obtained (a) after chemical cleaning of the Si (111) surface, (b) after thermal cleaning of the Si (111) surface, and (c) after Be deposition on Si (111) surface at 200 °C. (d) Schematic diagram of atomic arrangement between Be atoms and Si (111) surface.

arrangement, the lattice of Be layer rotates 30 degree around the normal of Si (111) surface with respect to the lattice of Si substrate, and the perfect lattice coincidence between Be layer and Si substrate occurs both along Si $\langle 11\bar{2} \rangle$ and $\langle 10\bar{1} \rangle$ directions with a ratio of 1:1 and 3:1, respectively. If there is no 30 degree rotation, the lattice mismatch will be:

$$f = \frac{a_{Be} - a_{Si(111)}}{a_{Si(111)}} = \frac{2.286 - 3.840}{3.840} = -40.5\%.$$

However, in our case, the lattice of Be layer rotates 30 degree around the normal of Si (111) surface with respect to the lattice of Si substrate, so the lattice mismatch will be:

$$f = \frac{a_{Be} \times \sqrt{3} - a_{Si(111)}}{a_{Si(111)}} = \frac{2.286 \times 1.732 - 3.840}{3.840} = 3.1\%.$$

Thus, the mismatch between the epitaxial layer and the substrate would be reduced from ~ -40.5 to $\sim 3.1\%$, greatly favoring the epitaxial growth of a high-quality Be layer on Si (111) with low defect density.

To find out the optimal conditions for Be deposition and the subsequent *in situ* oxidation process, a series of 5 nm Be thin layers were deposited on the chemically and thermally cleaned Si (111) surface at a substrate temperature ranging from room temperature (RT) to 500 °C with a constant Be beam flux. The *in situ* oxidation was performed at the same temperature as that of Be deposition. Figure 2a–f are the *in situ* RHEED patterns depicting the crystal structure evolutions during Be deposition and oxidation. It can be seen that the RHEED patterns of the Be layers become sharper and brighter from Fig. 2a to f, implying an improved crystal quality of the as-deposited Be layer. After *in situ* oxidation process, the RHEED patterns turn to obscure and disperse at RT and 100 °C (see Fig. 2a and b), indicating these films are highly strained with poor crystallinity. When the oxidation temperature rises to as high as 200 °C, the crystallinity of the BeO TL improves significantly as illustrated by the much clearer RHEED patterns with high contrast (see Fig. 2c). When oxidizing the Be layer at temperatures higher than 300 °C, although the RHEED patterns are still clear and

streaky, a new set of patterns appear at the azimuth of BeO $\langle 10\bar{1}0 \rangle$ (see Fig. 2d–f), suggesting the surface morphology is quite different from those samples oxidized at temperatures below 300 °C, which will be explained later on. It is worth to note that compared with other metals like Mg [7] and Sr [1], the deposition temperature of Be is relatively higher. No SiO_x or silicates or silicides are observed at the interface even at such high temperature, which is further confirmed by high-resolution transmission electron microscopy (HRTEM) and XPS results.

To study the influence of Be deposition temperature on the surface morphology, AFM measurements were carried out on two different samples with the Be layers deposited at 200 °C (sample A) and 500 °C (sample B), respectively. Figure 3a shows the AFM result of sample A where Si surface is fully covered by the continuous metal grains. The root mean square (rms) roughness in a $10 \times 10\ \mu m^2$ scanning area is about 0.88 nm (not shown here), demonstrating a high crystal quality and smooth surface, which is consistent with the *in situ* RHEED observations. After the *in situ* oxidation of sample A, the surface morphology still keeps the same features of the metal layer (see Fig. 3b) with a rms roughness of 0.67 nm in a $10 \times 10\ \mu m^2$ scanning area (not shown here), indicating the efficient protection of the Si surface by the Be thin layer. In contrast, the surface morphology of sample B is quite different with distinct metal islands (see Fig. 3c), showing a typical Volmer–Weber growth mode. At a higher substrate temperature, the mean free path of the Be atoms becomes longer together with the fact that Be–Be bonding is stronger than Be–Si bonding, resulting in an island surface structure. This surface morphology is consistent with the *in situ* RHEED results, where some bright spots can be clearly seen. On such an islanded surface, oxygen atoms could oxidize the Be metal layer not only in the normal direction but also in other side-directions, leading to multi-orientations in the BeO layer. This explains the appearance of the new set of RHEED patterns along the azimuths of $\langle 10\bar{1}0 \rangle_{BeO}$ in Fig. 2d–f. Therefore, combining the AFM and *in situ* RHEED results, the optimal temperature to synthesize crystalline and flat BeO TL is around 200 °C.
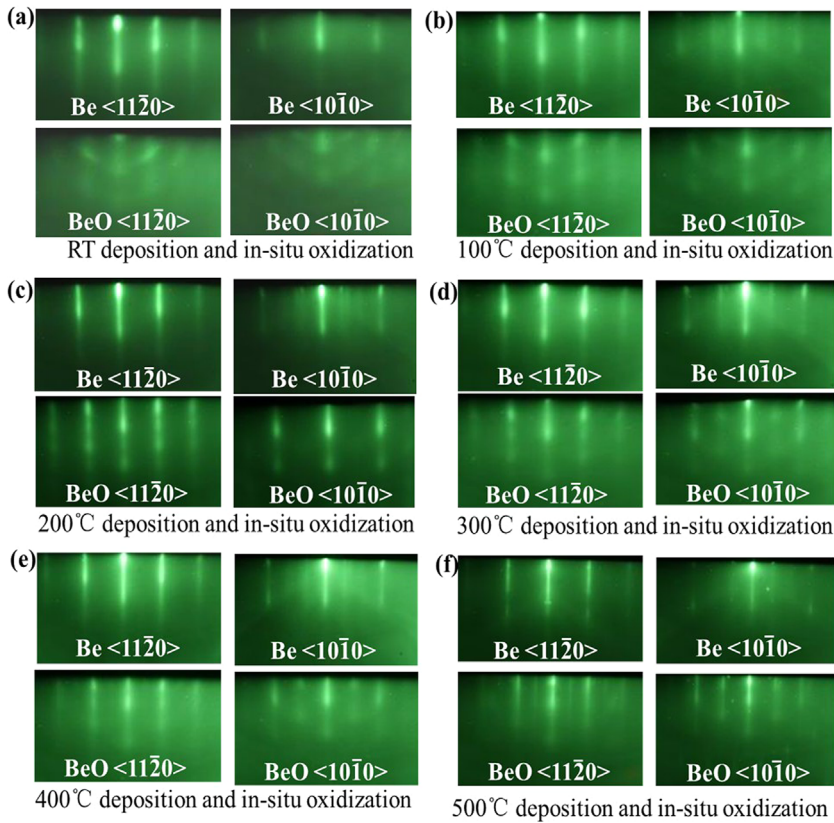
Figure 2 RHEED patterns with incident electron beams along $\langle 11\bar{2}0 \rangle_{Be}$ and $\langle 10\bar{1}0 \rangle_{Be}$ azimuths, respectively, obtained from Be deposition and corresponding *in situ* oxidation at (a) room temperature, (b) 100 °C, (c) 200 °C, (d) 300 °C, (e) 400 °C, and (f) 500 °C.

The interface structure was further analyzed by using the cross-sectional HRTEM. In order to protect the BeO TL during the thinning procedure, a ZnO capping layer with thickness of ∼350 nm was *in situ* deposited on BeO at 650 °C and then annealed at 750 °C in an oxygen radical environment for 10 min. Figure 4a–c show the results taken along $\langle 10\bar{1} \rangle_{Si}$ direction and its corresponding fast Fourier transformation (FFT) images. A well-defined interfacial layer can be obviously seen between ZnO capping layer and Si substrate from Fig. 4a, indicating the thermally and chemically stable BeO/Si interface even after a high temperature annealing. Figure 4b combined with Fig. 4a illustrates a wurtzite BeO phase and a crystalline orientation relationship of BeO [10$\bar{1}$0] //Si [10$\bar{1}$], agreeing well with the *in situ* RHEED observations. Figure 4d shows the HRTEM image of the interface along $\langle 10\bar{2} \rangle_{Si}$. An obvious interfacial layer between ZnO capping layer and Si substrate can also be clearly discerned. Figure 4e, which is the Fourier-filtered image of a part of Fig. 4d, suggests that the integrity of BeO (11$\bar{2}$0) planes is disturbed for almost every fifth planes, revealing that the interface has formed a coincidence lattice as reported [20]. Considering the 30° in-plane rotation of the BeO layer with respect to the Si substrate, the ratio

$$\frac{m}{n} = \frac{a_{BeO} \times \sqrt{3}}{a_{Si(111)}} = \frac{2.698 \times \sqrt{3}}{3.840} = \frac{6}{5} + \frac{1}{50}.$$

Since m and n are integers, we can take the ratio as

$$\frac{m}{n} \approx \frac{6}{5},$$

meaning that almost every six Si $(11\bar{2})$ planes will be coincident with every five BeO $(11\bar{2}0)$ planes, which is consistent with the observation in Fig. 4e. Further, the deviation parameter

$$F_0 = \frac{m a_{Si(111)} - n a_{BeO} \times \sqrt{3}}{m a_{Si(111)}}$$
$$= \frac{6 \times 3.840 - 5 \times 2.698 \times \sqrt{3}}{6 \times 3.840} = -1.4\%$$

can be obtained taking $m = 6$ and $n = 5$, implying that the in-plane lattice of BeO is under a compressive strain because of the influence from the Si substrate. As the distance away from the BeO/Si interface increases, the compressive strain in the BeO layer could be partially released.

This interface engineering technique with BeO transitional layers enables to monolithically integrate crystalline ZnO related materials on Si. A series of ZnO-based devices, including solar-blind ultraviolet photodetectors [21], dual-band ultraviolet photodetectors [22], heterojunction field effect transistors [23], and three terminal ultraviolet photodetectors [24] have been successfully built on Si substrates.

Rapid Research Letter

Phys. Status Solidi RRL 11, No. 5 (2017) (5 of 8) 1600443
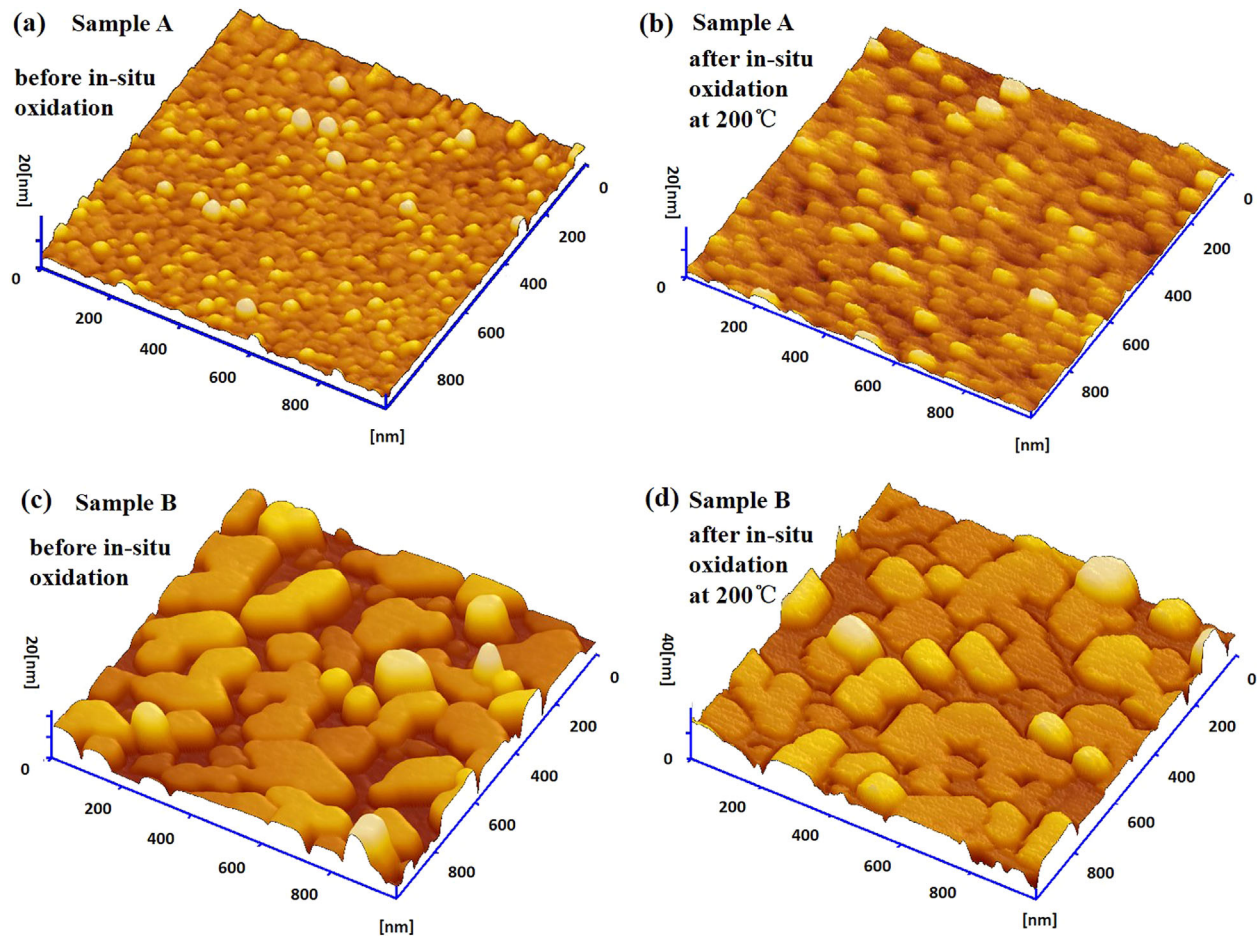
Figure 3 AFM images of the Be and BeO layers in a $1 \times 1\ \mu m^2$ scanning area: (a) after Be deposition at 200 °C, (b) after *in situ* oxidation of the Be layer at 200 °C, (c) after Be deposition at 500 °C, and (d) after *in situ* oxidation of the Be layer at 200 °C.

3.2 Crystalline BeO layer as a diffusion barrier against oxygen on Si

To evaluate the effectiveness of BeO as a diffusion barrier to protect Si surface from oxidation during the subsequent oxide growth, a 10 nm crystalline BeO layer was homoepitaxially grown on the above-described BeO TL. XRD θ–2θ and φ-scans were performed in the grazing incidence mode since the BeO layer is so thin compared with Si substrate that it is difficult to detect any signals coming from BeO under the normal incidence mode. Figure 5a shows the φ-scan result of BeO $(10\bar{1}0)$ plane carried out at around $\chi = 0.1°$ (the angle between the incident X-ray beam and the (0001) surface of the sample) and $2\theta = 38.12°$ (the Bragg angle based on the BeO $(10\bar{1}0)$ plane, which is consistent with the PDF card #35-0818). Six peaks show up with 60° apart, indicating a common sixfold symmetry of a wurtzite crystal structure, consistent with the *in situ* RHEED and *ex situ* HRTEM observations. Figure 5b shows the θ–2θ scans with different incident angles. According to the following equation

$$\alpha_C = \lambda \left(\frac{N_A r_e \rho Z}{\pi A} \right)^{\frac{1}{2}}$$

(λ is the wavelength of the incident X-ray beam, N_A is the Avogadro's constant, r_e is the classical electron radius, ρ, Z, and A denote the mass density, the effective atom number and the effective weight for material, respectively) [25], the critical grazing incident angle of the X-ray beam in the BeO layer was calculated as about 0.25°, above which the penetration depth will increase sharply as the incident angle increases. As shown in Fig. 5b, the Bragg angle of the BeO $(10\bar{1}0)$ plane decreases from 38.26° to 38.10° when decreasing the penetration depth, implying that the in plane lattice parameter along the direction of BeO $\langle 10\bar{1}0 \rangle$ increases from BeO/Si interface to the BeO surface. This variety means that the compressive strain in the BeO layer is gradually released, in accordance with the result shown in Fig. 4e.

High-resolution XPS spectrum shown in Fig. 6 confirms the effectiveness of BeO as an oxygen diffusion barrier. A sample using low-temperature interface engineering technique with the Mg and MgO TL was also prepared for a comparison (the growth details can be found in Ref. [7]). The schematic structures of the two samples are shown in the inset. For clarity, the data was normalized according to the intensity of $Si^0 2p$ of the two samples. For the sample
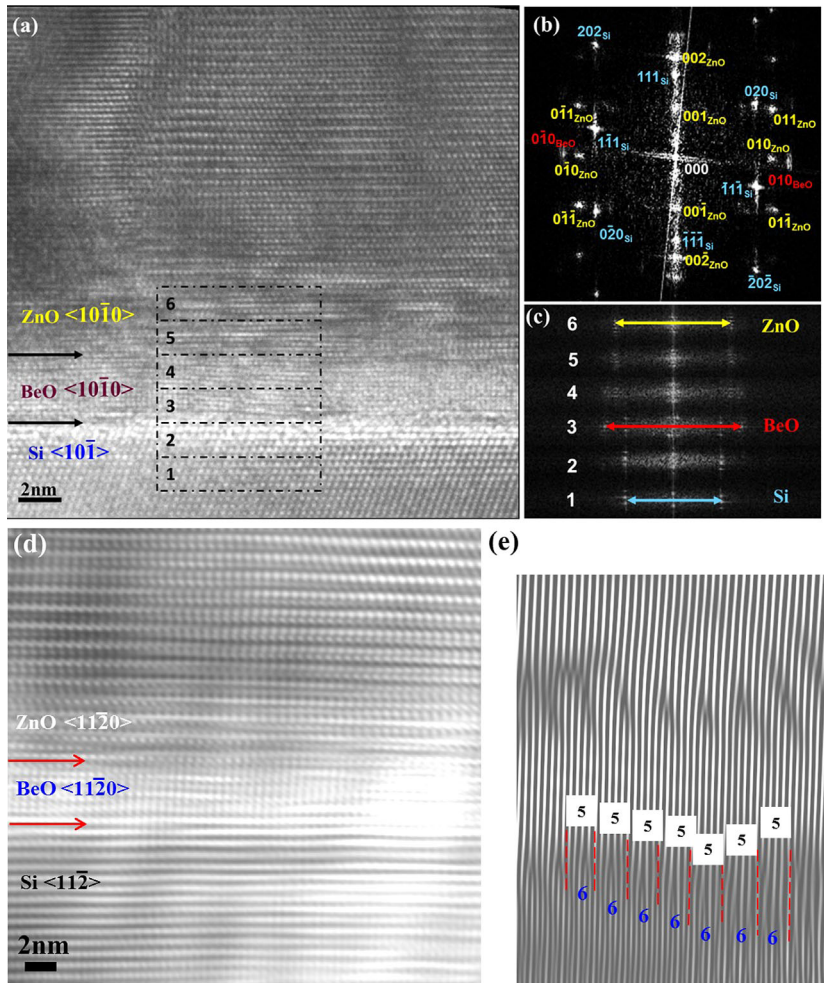
Figure 4 (a) Cross-sectional HRTEM micrograph along $\langle 10\bar{1}\rangle_{Si}$ direction near the interface region, (b) FFT pattern from the whole observed area, (c) corresponding FFT patterns obtained from different layers as indicated by the numbers in (a). (d) Cross-sectional HRTEM micrograph along $\langle 11\bar{2}\rangle_{Si}$ direction near the interface region, (e) a fraction from the filtered FFT pattern of the whole corresponding area observed in (d).

using MgO TL combined with 15 nm MgO layer, a little content of SiO_2 is detected, indicating oxygen atoms diffuse from MgO to reach Si. In contrast, there are only two peaks corresponding to Si 2p in element state (about 99 eV) and Be 1s in oxidation state (about 113.67 eV) [26] in the sample using BeO TL combined with 10 nm BeO layer. Compared with the previous report using ALD-grown BeO layer where some little content Si-O peak appears [27], no signal related

with Si in other chemical state is detected in our sample, suggesting that these combined BeO layers can sufficiently stop the oxygen atoms' diffusion even though the whole growth and *in situ* annealing processes were carried out under the active oxygen radicals at high temperature. This clear and sharp interface without formation of SiO_2 could increase the gate stack capacitance, which is desired for further scaling the devices on Si.
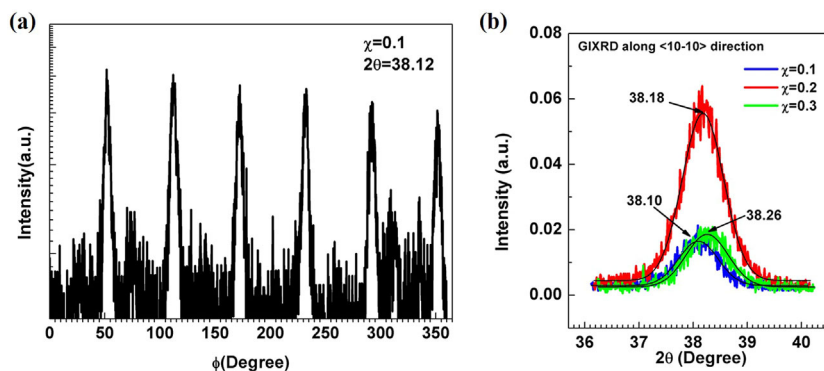
Figure 5 (a) GIXRD ϕ-scan of wurtzite BeO $(10\bar{1}0)$ plane, (b) GIXRD θ–2θ scan of wurtzite BeO $(10\bar{1}0)$ plane at different incident angles.

Phys. Status Solidi RRL 11, No. 5 (2017)

Rapid
Research Letter

(7 of 8) 1600443
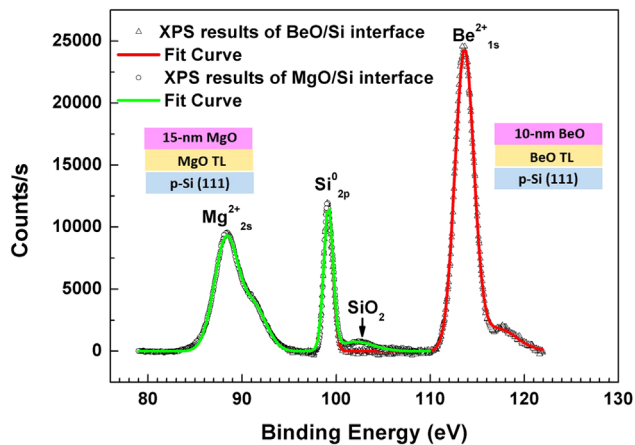
Figure 6 High-resolution XPS spectrum at the interface of BeO/Si and MgO/Si.

3.3 Crystalline BeO layer as an insulator layer A 70 nm BeO layer was homo-epitaxially grown on above-described BeO TL and a 130 nm ZnO layer was deposited subsequently to serve as an active channel layer. Figure 7a is the *in situ* RHEED observations, indicating that both crystalline BeO and ZnO are successfully achieved. Figure 7b is the result of cross-sectional scanning electron microscopy (SEM), from which we can clearly see the thickness of both BeO and ZnO layers. High resolution XRD curves obtained by synchrotron radiation in Fig. 7c and d further confirm the crystalline nature of these two layers. A BG-TFT device is fabricated using the ZnO (130 nm)/BeO (70 nm)/Si structure to evaluate the feasibility of the crystalline BeO layer as the gate insulator. The device performs a normal transistor behavior as shown in Fig. 8a and b. It can be found the turn-on voltage of the device is close to 1 V. Thus, the TFT device clearly works in the enhancement mode, indicating that ZnO channel layer has very low background electron concentration and the quality of ZnO film seems to be good, which is a great advantage of single crystal ZnO channel layer and could be hardly realized on polycrystalline counterparts. The subthreshold slope (S.S.) is deduced as 0.8 V/decade and field effect mobility as $2.13 \, \mathrm{cm^2 \, V^{-1} \, s^{-1}}$, which are not in the state of the art. This turn-on characteristic is mainly due to the defects at ZnO/BeO interface, which originate from the large lattice misfit between ZnO ($a = 3.249 \, \text{Å}$) and BeO ($a = 2.698 \, \text{Å}$). Further modification should be carried out to improve the device performance.

4 Conclusions In summary, we have systematically investigated the *in situ* oxidation process of the Be layer deposited on Si (111) surface by MBE technique using *in situ* RHEED monitoring combined with *ex situ* AFM and HRTEM observations. A high-quality interface between single wurtzite BeO TL and Si substrate has been realized, which can serve as a template for the following COS growth. A 10 nm single crystal BeO layer was homo-epitaxially grown on the BeO TL confirmed by GIXRD measurement and can totally block the diffusion of active oxygen atoms during the whole growth procedure even after a high temperature annealing at 750 °C. At last, a BG-TFT working in the enhancement mode was achieved using the structure of ZnO (130 nm)/BeO (70 nm)/Si, demonstrating it is a potential alternative to SiO₂ and that this methodology can
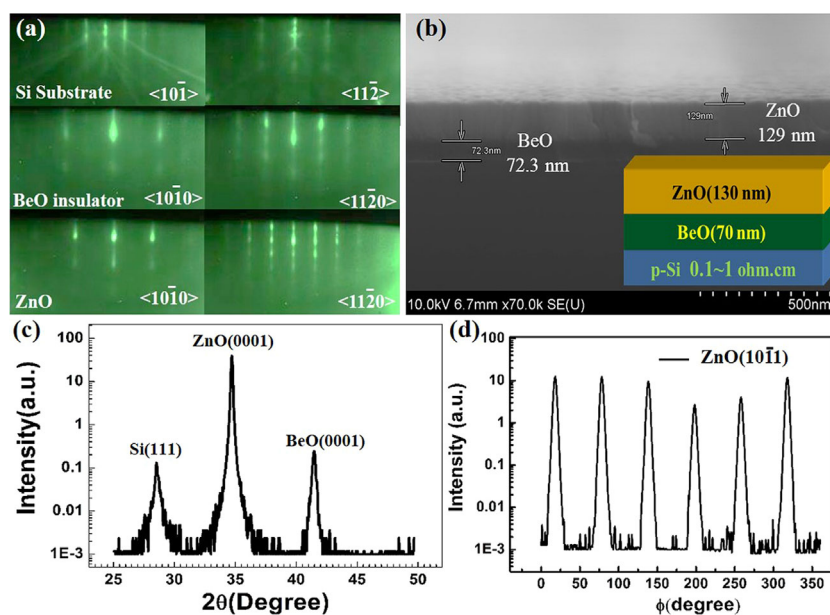
Figure 7 (a) RHEED patterns of Si, BeO, and ZnO layers along the $\langle 11\bar{2} \rangle_{Si}$ and $\langle 10\bar{1} \rangle_{Si}$ azimuths, respectively. (b) Cross-sectional SEM image of ZnO/BeO/Si heterostructure. (c) XRD θ–2θ scan of ZnO (002) plane, (d) XRD ϕ-scan of ZnO (10$\bar{1}$1) plane.
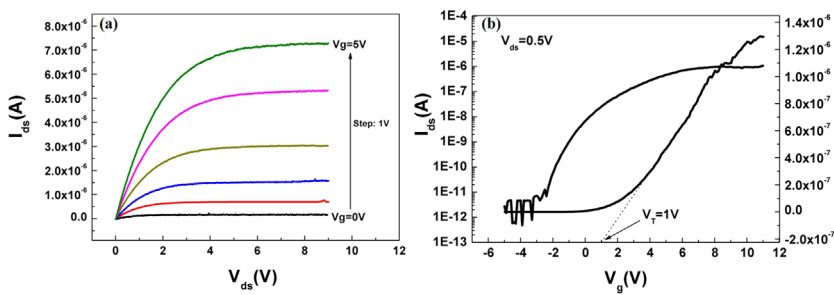
Figure 8 (a) Output *I–V* curve of BG-TFT on ZnO/BeO/Si, (b) transfer *I–V* curve of BG-TFT on ZnO/BeO/Si.

be potentially extended to combine other technologically important crystalline oxides such as ZnO related materials with the well-developed Si infrastructures.

References

[1] J. W. Reiner, A. M. Kolpak, Y. Segal, K. F. Garrity, S. Ismail-Beigi, C. H. Ahn, and F. J. Walker, Adv. Mater. **22**, 2919 (2010).

[2] J. M. Vila-Fungueiriño, R. Bachelet, G. Saint-Girons, M. Gendry, M. Gich, J. Gazquez, E. Ferain, F. Rivadulla, J. Rodriguez-Carvajal, N. Mestres, and A. Carretero-Genevrier, Front. Phys. **3**, 38 (2015).

[3] S. R. Bakaul, C. R. Serrao, M. Lee, C. W. Yeung, A. Sarker, S. L. Hsu, A. K. Yadav, L. Dedon, L. You, A. I. Khan, J. D. Clarkson, C. Hu, R. Ramesh, and S. Salahuddin, Nature Commun. **7**, 10547 (2016).

[4] A. Carretero-Genevrier, M. Gich, L. Picas, J. Gazquez, G. L. Drisko, C. Boissiere, D. Grosso, J. Rodriguez-Carvajal and C. Sanchez, Science **340** (6134), 827 (2013).

[5] H. J. Osten, A. Laha, M. Czernohorsky, E. Bugiel, R. Dargis, and A. Fissel, Phys. Status Solidi A **205**, 695 (2008).

[6] R. A. McKee, F. J. Walker, and M. F. Chisholm, Phys. Rev. Lett. **81**, 3014 (1998).

[7] X. N. Wang, Y. Wang, Z. X. Mei, J. Dong, Z. Q. Zeng, H. T. Yuan, T. C. Zhang, and X. L. Du, Appl. Phys. Lett. **90**, 151912 (2007).

[8] V. Shutthanandan, S. Thevuthasan, Y. Liang, E. M. Adams, Z. Yu, and R. Droopad, Appl. Phys. Lett. **80**, 1803 (2002).

[9] L. Zhang and R. Engel-Herbert, Phys. Status Solidi RRL **8**, 917 (2014).

[10] J. Zhang, G. T. Stauf, R. Gardiner, P. Van Buskirk, and J. Steinbeck, J. Mater. Res. **9**, 1333 (1994).

[11] C. Merckling, M. El-Kazzi, G. Delhaye, M. Gendry, G. Saint-Girons, G. Hollinger, L. Largeau, and G. Patriarche, Appl. Phys. Lett. **89**, 232907 (2006).

[12] H. J. Osten, M. Czernohorsky, R. Dargis, A. Laha, D. Kühne, E. Bugiel, and A. Fissl, Microelectron. Eng. **84**, 2222 (2007).

[13] D. O. Klenov, L. F. Edge, D. G. Schlom, and S. Stemmer, Appl. Phys. Lett. **86**, 051901 (2005).

[14] Z. Pan, Y. Du, B. Huang, H. H. Xu, Y. Liu, H. L. Chen, W. Xiong, and R. Schmid-Fetzer, J. Mater. Sci. **41**, 2525 (2006).

[15] K. J. Hubbard and D. G. Schlom, J. Mater. Res. **11**, 2757 (1996).

[16] J. H. Yum, T. Akyol, M. Lei, D. A. Ferrer, T. W. Hudnall, M. Downer, C. W. Bielawski, G. Bersuker, J. C. Lee, and S. K. Banerjee, J. Cryst. Growth **334**, 126 (2011).

[17] J. H. Yum, T. Akyol, M. Lei, T. Hudnall, G. Bersuker, M. Downer, C. Bielawski, J. Lee, and S. Banerjee, J. Appl. Phys. **109**, 064101 (2011).

[18] C. Andeen, D. Schuele, and J. Fontanella, J. Appl. Phys. **45**, 1071 (1974).

[19] M. Lei, J. H. Yum, J. Price, T. Hudnall, C. Bielawski, S. Banerjee, P. Lysaght, G. Bersuker, and M. Downer, Appl. Phys. Lett. **100**, 122906 (2012).

[20] A. Trampert and K. H. Ploog, Cryst. Res. Technol. **35**, 793 (2000).

[21] H. L. Liang, Z. X. Mei, Q. H. Zhang, L. Gu, S. Liang, Y. N. Hou, D. Q. Ye, C. Z. Gu, R. C. Yu, and X. L. Du, Appl. Phys. Lett. **98**, 221902 (2011).

[22] Y. N. Hou, Z. X. Mei, H. L. Liang, D. Q. Ye, C. Z. Gu, and X. L. Du, Appl. Phys. Lett. **102**, 153510 (2013).

[23] D. Q. Ye, Z. X. Mei, H. L. Liang, J. Q. Li, Y. N. Hou, C. Z. Gu, A. Azarov, A. Kuznetsov, W. C. Hong, Y. C. Lu, and X. L. Du, J. Phys. D: Appl. Phys. **47**, 255101 (2014).

[24] D. Q. Ye, Z. X. Mei, H. L. Liang, L. S. liu, Y. H. Zhang, J. Q. Li, Y. P. Liu, C. Z. Gu, and X. L. Du, Sci. Rep. **6**, 26169 (2016).

[25] W. S. Tan, H. L. Cai, X. S. Wu, S. S. Jiang, W. L. Zheng, and Q. J. Jia, J. Alloys Compd. **397**, 231 (2005).

[26] G. Soto, J. A. Díaz, R. MAchorro, A. Reyes-Serrato, and W. de la Cruz, Mater. Lett. **52**, 29 (2002).

[27] J. H. Yum, G. Bersuker, T. Akyol, D. A. Ferrer, M. Lei, K. W. Park, T. W. Hudnall, M. C. Downer, C. W. Bielawski, E. T. Yu, J. Price, J. C. Lee, and S. K. Banerjee, IEEE Trans. Electron Devices **58**, 4384 (2011).